Multi-User Indoor Optical Wireless Communication System Channel Control Using A Genetic Algorithm

Matthew D. Higgins, Roger J. Green, Mark S. Leeson, Evor L. Hines

m.higgins@warwick.ac.uk; roger.green@warwick.ac.uk; mark.leeson@warwick.ac.uk; e.l.hines@warwick.ac.uk

All authors are with the:-

School of Engineering, University of Warwick, Coventry, CV4 7AL, UK.

First Submission Date: 12-03-2010

Revision Submission Date: 19-07-2010

Keywords: optical communications, optical wireless, genetic algorithm, wireless LAN, mobile communications

Abstract

A genetic algorithm controlled multispot transmitter is demonstrated that is capable of optimising the received power distribution for randomly aligned single element receivers in multiple fully diffuse optical wireless communications systems with multiple mobile users. Using a genetic algorithm to control the intensity of individual diffusion spots, system deployment environment changes, user movement and user alignment can be compensating for, with negligible impact on

the bandwidth and RMS delay spread. It is shown that the dynamic range, referenced against the peak received power, can be reduced by up to 27% for empty environments and by up to 26% when the users are moving. Furthermore, the effect of user movement, that can perturb the channel by up to 8%, can be reduced to within 5% of the optimised case. Compared to alternative bespoke designs that are capable of mitigating optical wireless channel drawbacks, this method provides the possibility of cost-effectiveness for mass-produced receivers in applications where end-user friendliness and mobility are paramount.

1 Introduction

Indoor optical wireless (OW) communications using an infrared (IR) carrier provides traits of mobility found in the radio frequency (RF) domain with the advantageous high bandwidth availability of the optical domain [1]. One of the most challenging design aspects of an indoor OW system, however, is overcoming the limitations imposed by the channel, for which the characteristics are dependent upon the room size, stationary and moving objects, material properties of every surface upon which the radiation is incident, and the number and type of illumination sources present [2,3]. This, essentially infinite, level of channel variability implies a single system design may have different performance capabilities when deployed in different environments, inhibiting the ability to provide high performance OW systems that meet the needs of today's growing demand for mobile multimedia device connectivity.

Proceeding from the pioneering work by Gfeller and Bapst [4], several solutions have been proposed that mitigate the channel's influence on system performance. Quasi-diffuse configurations, employing multispot diffusion (MSD) and diversity receivers [5], ameliorate the bandwidth and

ambient noise rejection through the use of an array of photodetectors coupled to either a single imaging lens [6], or several optical concentrators [7]. Modulation techniques, such as trellis-coded pulse-position modulation [8], and amplitude shift keying digital demodulation [9], are capable of overcoming the effects of intersymbol interference (ISI), and cyclostationary noise from fluorescent lamps [3], respectively. It has also been shown that the use of so-called *intelligent* techniques could be beneficial. In [10] a combined neural network with pattern recognition wavelet analysis was used to overcome channel induced distortion [10], whilst in [11, 12] a modified genetic algorithm (GA), based on simulated annealing [13], was shown to produce highly optimised computer generated holograms, reducing the variation in received power distribution.

The most practical OW system deployment architecture is cellular, where a given room or section of a room, has a transceiver base station linking multiple battery-powered OW devices to the primary backbone network. Therefore, whilst the implementation of any of the aforementioned techniques has certain performance merits compared to a conventional diffuse system, the increased cost, complexity and physical size of each receiver must be considered. This becomes an increasingly more apparent factor when the number of receivers increases, as the overall system cost will be influenced more by the number of receivers than by an individual base station.

A recent solution to this issue was proposed, based upon a GA controlled MSD transmitter, but where the traditionally employed diversity receiver was replaced by a simpler single element receiver [14, 15]. By using the GA to control the intensity of individual spots, similar received power distributions, with a negligible bandwidth and RMS delay spread penalty, could be formed in multiple rooms, independent of the reflectivity characteristics and single user movement patterns. The adaptability provided the possibility of implementing a simpler receiver, as

the transmitter became responsible for overcoming channel variability. This initial work contained a major simplification in an assumption that the receivers were all vertically orientated, even whilst moving. A further study extended the ability of the GA to allow for user-induced random alignment variability with good success [16]. However, as previously mentioned, this GA technique becomes beneficial when the number of receivers becomes larger, for which, in this paper, the feasibility is shown to extend to multiple users, each with different movement patterns in multiple environments.

The remainder of this paper is organised as follows: Section 2 overviews the general system model and impulse response calculations, section 3 introduces the channel model theory followed by section 4 that covers the GA implementation. Section 5 provides the results and associated analysis, followed by concluding remarks in section 6.

2 System Model

2.1 Source, Receiver and Reflector Model

The system deployment environment is defined to be an arbitrary indoor rectangular room for which the surfaces exhibit a fully-diffuse reflection characteristic that can be described by Lambert's reflection model [17]. A diffusion spot geometry is formed on the ceiling of the room using either multiple optical sources [18], or a 2-D array of either vertical cavity surface emitting Laser diodes (VCSELs), or resonant cavity LEDs (RCLEDs) [19, 20]. For the case of multiple optical sources, the emitted radiation profile can be controlled via lenses or other diffuser techniques [21], but typically the source is an LED which emits radiation with a generalised Lambertian radiation intensity pattern [22]. From a receiver point of view, abstracting the method used to generate the

spots allows for each of I diffusion spots on the ceiling to be considered as independent sources $\mathcal{S}_i$, since either the reflected radiation from a 2-D VCSEL/RCLED array or independent sources appears identical. The only error accompanying this assumption is a delay and propagation loss between the emitting element of a 2-D VCSEL/RCLED array and the diffusion spot position. However, it allows for a simplification of the argument towards using the GA, whilst maintaining generality in the application, independent of the technique used for diffusion spot generation.

Referring to Figure 1, each source, $\mathcal{S}_i$, will have an associated position vector $\mathbf{r}_{\mathcal{S}_i}$, unit length orientation vector $\hat{\mathbf{n}}_{\mathcal{S}_i}$, power $P_{\mathcal{S}_i}$ and uniaxial symmetric (with respect to $\hat{\mathbf{n}}_{\mathcal{S}_i}$) Lambertian radiation intensity profile $R(\phi)$ given by

$$R(\phi) = \frac{n+1}{2\pi} P_{\mathcal{S}_i} \cos^n(\phi) \qquad \text{for } \phi \in [-\pi/2, \pi/2] \tag{1}$$

where the mode number, $n = 1$, for a pure Lambertian diffuser, such as the ceiling, and $n > 1$ for a diffusion spot from an LED with higher directionality.

For a given environment, the existence of $J = 1024$ identical single element receivers $\mathcal{R}_j$, uniformly distributed over the width x, length y, at a height $z = 1\,\text{m}$, is modelled. Each receiver has a position vector $\mathbf{r}_{\mathcal{R}_j}$, orientation vector $\hat{\mathbf{n}}_{\mathcal{R}_j}$, active optical collection area $A_{\mathcal{R}_j}$ and a field of view $\text{FOV}_{\mathcal{R}_j}$, defined as the maximum uniaxial symmetric incident angle of radiation with respect to $\hat{\mathbf{n}}_{\mathcal{R}_j}$ that will generate a current in the photodiode. Furthermore, according to previously published work into the effects of mobile receiver alignment statistics on system performance [16], the orientation in the x and y axis of each receiver is derived from a normal distribution with mean $\bar{z} = 0$ (no rotation), and standard deviation $\sigma = 11.7$, providing a respective 0.8 probability of rotation within $\pm 15°$, and 0.99 within $\pm 30°$ from the unrotated case in each axis.

Under the assumption that all surfaces exhibit Lambertian reflection characteristics, the technique described in [23] can be employed, whereby the surfaces are partitioned into L elements $\mathcal{E}_l$, with position vector $\mathbf{r}_{\mathcal{E}_l}$, orientation vector $\hat{\mathbf{n}}_{\mathcal{E}_l}$, and size $A_{\mathcal{E}_l} = 1/\Delta A^2(\mathrm{m}^2)$, where ΔA is the desired number of elements per metre. A given element will behave sequentially, firstly as a receiver $\mathcal{E}_l^{\mathcal{R}}$ with a hemispherical FOV, for which the received power $P_{\mathcal{E}_l}$ can be determined, and secondly as a source $\mathcal{E}_l^{\mathcal{S}}$, with a radiation intensity profile $R(\phi)$ as given by (1) setting $n = 1$ and $P_{\mathcal{S}_i} = \rho_{\mathcal{E}_l} P_{\mathcal{E}_l}$, where $\rho_{\mathcal{E}_l}$ is the reflectivity of the element determined by its respective material properties.

2.2 Impulse Response Calculations

The IR radiation incident upon a receiver $\mathcal{R}_j$ will be the result of the radiation emitted from a source $\mathcal{S}_i$ that has propagated directly through an unobstructed line of sigth (LOS) path, and/or from the radiation that has undergone a finite number, k, reflections off the surfaces within the environment. It is also known [17,23] that, in an intensity modulation, direct detection (IM/DD) channel, where the movement of transmitters, receivers or objects in the room is slow compared to the bit rate of the system, no multipath fading occurs, and, as thus the channel, can be deemed linear time invarient (LTI). The impulse response $h(t; \mathcal{S}_i, \mathcal{R}_j)$ is given by [23, 24]

$$h(t; \mathcal{S}_i, \mathcal{R}_j) = \sum_{k=0}^{k} h^k(t; \mathcal{S}_i, \mathcal{R}_j) \tag{2}$$

where $h^k(t; \mathcal{S}_i, \mathcal{R}_j)$ is the impulse response of the system for radiation undergoing k reflections between $\mathcal{S}_i$ and $\mathcal{R}_j$.

To determine the impulse response, it is assumed that each source $\mathcal{S}_i$ emits a unit impulse

($P_{\mathcal{S}_i} = 1\,\mathrm{W}$) at $t = 0$, such that the LOS ($k = 0$) impulse response is given by the scaled and delayed Dirac delta function

$$h^0(t; \mathcal{S}_i, \mathcal{R}_j) \approx R(\phi_{ij}) \frac{\cos(\theta_{ij}) A_{\mathcal{R}j}}{D_{ij}} V(\frac{\theta_{ij}}{\mathrm{FOV}_{\mathcal{R}j}}) \delta(t - \frac{D_{ij}}{c}) \tag{3}$$

Where, referring to Figure 1, $D_{ij} = ||\mathbf{r}_{\mathcal{S}_i} - \mathbf{r}_{\mathcal{R}_j}||$ is the distance between source and receiver, c is the speed of light; ϕ_{ij} and θ_{ij} are the angles between $\hat{\mathbf{n}}_{\mathcal{S}_i}$ and $(\mathbf{r}_{\mathcal{R}_j} - \mathbf{r}_{\mathcal{S}_i})$, and between $\hat{\mathbf{n}}_{\mathcal{R}_j}$ and $(\mathbf{r}_{\mathcal{S}_i} - \mathbf{r}_{\mathcal{R}_j})$, respectively. $V(x)$ represents the the visibility function, where $V(x) = 1$ for $|x| \leq 1$, and $V(x) = 0$ otherwise.

For radiation undergoing $k > 0$ bounces, the impulse response is given by

$$h^k(t; \mathcal{S}_i, \mathcal{R}_j) = \sum_{l=1}^{L} h^{(k-1)}(t; \mathcal{S}_i, \mathcal{E}_l^{\mathcal{R}}) * h^0(t; \mathcal{E}_l^{\mathcal{S}}, \mathcal{R}_j) \tag{4}$$

where $*$ denotes convolution, and the $(k-1)$ impulse response $h^{(k-1)}(t; \mathcal{S}_i, \mathcal{E}_l^{\mathcal{R}})$ can be found iteratively [24] from

$$h^k(t; \mathcal{S}_i, \mathcal{E}_l^{\mathcal{R}}) = \sum_{l=1}^{L} h^{(k-1)}(t; \mathcal{S}_i, \mathcal{E}_l^{\mathcal{R}}) * h^0(t; \mathcal{E}_l^{\mathcal{S}}, \mathcal{E}_l^{\mathcal{R}}) \tag{5}$$

where all the zero order ($k = 0$), responses in (4) and (5) are found by careful substitution of the variables in (3). Due to the computational time required for this iteratative calculation being proportional to k^2 [25], the simulations will firstly be limited to the third order impulse response ($k = 3$), and secondly the segmentation resolution of the environment is changed for each reflection, setting $\Delta A_1 = 20$, $\Delta A_2 = 6$ and $\Delta A_3 = 2$. It should also be noted that the resultant impulse response in (2) will produce a finite sum of scaled delta functions which need to undergo temporal smoothing, by subdividing time into bins of width Δt, and summing the total power in each bin [23]. For this work, a single time bin width of $\Delta t = 0.1\,\mathrm{ns}$ is assumed.

3 The Channel Model

For a nondirected IR channel employing IM/DD, a source $\mathcal{S}_i$, which emits an instantaneous optical power $X_i(t)$, will produce a instantaneous photocurrent $Y_{ij}(t)$ at receiver $\mathcal{R}_j$ with photodiode responsivity r_j in the presence of an additive, white Gaussian shot noise $N_j(t)$, and can be modelled as a linear baseband system, given by [26]

$$Y_{ij}(t) = r_j X_i(t) * h(t; \mathcal{S}_i, \mathcal{R}_j) + N_j(t) \tag{6}$$

If all I sources $\mathcal{S}_i$ emit identical signal waveforms, $X_i(t) \forall i \in \{1, 2, \ldots, I\}$, but with individually scaled magnitudes, a_i, the instantaneous photocurrent at a given receiver $Y_j(t)$ is simply the summation of (6) for all sources

$$Y_j(t) = \sum_{i=1}^{I} (r_j a_i X_i(t) * h(t; \mathcal{S}_i, \mathcal{R}_j)) + N_j(t) \tag{7}$$

Furthermore, through channel linearity, and knowing that r_j is identical for all receivers, a set of scaling factors a_i exist providing a solution to

$$\sum_{i=1}^{I} a_i h(t; \mathcal{S}_i, \mathcal{R}_1) \approx \sum_{i=1}^{I} a_i h(t; \mathcal{S}_i, \mathcal{R}_2) \approx \ldots \approx \sum_{i=1}^{I} a_i h(t; \mathcal{S}_i, \mathcal{R}_J) \tag{8}$$

Such that, by incorporation into (7), all of the J receivers will produce the same or very similar photocurrents

$$Y_1(t) \approx Y_2(t) \approx \ldots \approx Y_J(t) \tag{9}$$

Inspection of equations (7) to (9), implies a solution may require some scaling factors of ≤ 1, lowering the total received power, compared to if all sources were maximal. Furthermore, solving (9) for different environments, will yield non-identical sets of scaling factors, implying that the magnitude of the received power, although equal at all locations within the environment, will be different.

This can be compensated by drawing parallels with the IEEE 802.11a WiFi physical layer specification, that incorporates multi-rate transmission of up to 54Mbit/s [27], and recent work on rate-adaptive transmission [28] in the IR domains; if it is found that several environments have different received powers, the following method can be applied. Firstly, by normalising the I scaling factors, the equality result of (9) is independent of receiver power magnitude. Secondly, for different environments, we can adjust for example, the pulse characteristic, in order to increase or decrease the received power to make the power distributions equal. This then allows for the same optimal receiver design to be used in different environments, albeit under the compromise of variable data rates in the same manner as most other variable data rate systems.

To illustrate the final problem simplification applied, consider, for example, an environment, with dimensions $x = y = 6\,\mathrm{m}, z = 3\,\mathrm{m}$. In calculating a third order reflection impulse response ($k = 3$), the longest time of flight for the radiation to travel is $t = (4(6^2 + 6^2 + 3^2)^{0.5})/c \approx 120\,\mathrm{ns}$, when it undergoes a path reflecting off the opposite corners of the room. Using an impulse response bin width $\Delta t = 0.1\,\mathrm{ns}$ would produce 1200 samples for each impulse response train for every combination of I sources and J receivers in (8).

Proposing a GA that can solve (8) for the possibly infinite number of source and transmitter configurations would be too unwieldy. By replacing the need to evaluate each bin of the impulse response train with the need to find only the scaling factor solution for the time integral, or DC value of the frequency response, $H(0; \mathcal{S}_i, \mathcal{R}_j) = \int_{-\infty}^{\infty} h(t; \mathcal{S}_i, \mathcal{R}_j)dt$, equation (8) reduces to

$$\sum_{i=1}^{I} a_i H(0; \mathcal{S}_i, \mathcal{R}_1) \approx \sum_{i=1}^{I} a_i H(0; \mathcal{S}_i, \mathcal{R}_2) \approx \ldots \approx \sum_{i=1}^{I} a_i H(0; \mathcal{S}_i, \mathcal{R}_J) \tag{10}$$

Optimisation of the power distribution, however, should not be achieved at the expense of bandwidth and RMS delay spread. As (10) only quantifies the total power received, not when

it was received, the solution will be fed back into the original system model to quantify the worst case bandwidth and RMS delay spread, defined as the smallest and largest values at any location within the room, respectively. The RMS delay spread can be found from the original impulse response using [29]

$$\text{RMS Delay Spread} = \sqrt{\frac{\int_{-\infty}^{\infty}(t-\omega)^2 h^2(t)dt}{\int_{-\infty}^{\infty} h^2(t)dt}} \tag{11}$$

Where ω is defined as

$$\omega = \frac{\int_{-\infty}^{\infty} t h^2(t)dt}{\int_{-\infty}^{\infty} h^2(t)dt} \tag{12}$$

4 The Genetic Algorithm

GAs should be considered as a general framework that needs to be tailored to a specific problem [30]. A substantial review, evaluation and justification to the methodology used to adapt the representation, fitness function, selection, recombination and mutation sub-routines found in the so-called *canonical* GA was presented in [14]. In that paper, 2 algorithms, derived from over 200 possible permutations of the algorithms sub-routines was found to be suitable for this type of optimisation scenario. Furthermore, the 2 proposed algorithms were also shown to be successful when applied to incrementally more complex scenarios including random user alignment of the receivers [16]. The work presented here uses the same 2 GAs carefully developed there, so in the interest of conciseness, only a brief factual description will be provided here.

Firstly, the scaling factors $a_i \forall i \in \{1, \ldots, I\}$ are allowed to take on the values in the set $\{0, 0.01, \ldots, 1\}$, such that the search space $\Phi_g = \{0, 0.01, \ldots, 1\}^I$, will provide $|\Phi_g| = 101^I$ possible solutions [31]. These encoding values were chosen [14] such that there is a fine enough scale of possible powers that each of the spots can operate at, for example, the maximum scaling

factor of 1 indicates full power, whilst the minimum scaling factor of 0 would indicate the spot is off, where therefore values between will indicate single percentage increments between fully on and off. It should also be noted that the order of the encoding does have a bearing upon the GAs ability to produce a satisfactory optimisation, where as in Fig. 2 of [14], a concertina structure was shown to be effective for the algorithms under consideration. It is further defined that a population $\Psi(t)$ at time t, of μ solutions $\mathbf{a}_\nu = (a_1, \ldots, a_I) \in \Phi_g, \forall \nu \in \{1, \ldots, \mu\}$, exists.

At any given time t, each solution $\mathbf{a}_\nu$, is evaluated by the objective, or fitness function, F, which, for the results presented here, is given by

$$F(\mathbf{a}_\nu) = 100 - \left(100 \left(\frac{\max H(0;\mathbf{a}_\nu) - \min H(0;\mathbf{a}_\nu)}{\max H(0;\mathbf{a}_\nu)}\right)\right) \tag{13}$$

Where $\max H(0;\mathbf{a}_\nu)$ and $\min H(0;\mathbf{a}_\nu)$ are the maximum and minimum DC frequency responses for any receiver after application of the scaling factor solution $\mathbf{a}_\nu$ to the source powers. It can be seen that the fitness function measures the percentage change or deviation from the peak power in the room. A solution $\mathbf{a}_\nu$, whose source scaling factors produce a perfectly uniform power distribution, will have a fitness of 100%. Furthermore the global maximum optimal solution, $\hat{\mathbf{a}}_\nu$, is given by

$$\hat{\mathbf{a}}_\nu = \max_{\mathbf{a}_\nu \in \Phi_g} F(\mathbf{a}_\nu) \tag{14}$$

After evaluation of each possible solution $\mathbf{a}_\nu$ by the fitness function, some selection operator must be applied that emphasises the fitter solutions, such that they are passed onto the next generation [32]. In this work two, selection routines are used, namely, stochastic uniform sampling (SUS), and tournament selection. The SUS selection scheme assigns a probability of selection, p_ν^{prop}, proportional to an individual's relative fitness within the population, and is given by

$$p_\nu^{\text{prop}} = \frac{F(\mathbf{a}_\nu)}{\sum_{\nu=1}^{\mu} F(\mathbf{a}_\nu)} \tag{15}$$

The probabilities are then contiguously mapped onto a wheel, such that $\sum_{\nu=1}^{\mu} p_{\nu}^{\text{prop}} = 1$. Following the mapping, μ uniformly spaced numbers in the range $[0, 1]$ are offset by a singularly generated random number. Solutions for which the cumulative probability spans any of the μ numbers are selected for reproduction [33], and for the SUS selection presented here, $\mu = 200$.

Tournament selection is carried out by first ranking all solutions in the population $\Psi(t) = \{\mathbf{a}_1, \ldots, \mathbf{a}_\mu\}$ by their absolute fitness from (13), where $\mathbf{a}_1$ is the fittest, and $\mathbf{a}_\mu$ is the least. Then, μ times, q solutions are randomly selected for a tournament, where the fittest is selected for the next generation. The probability of a solution $\mathbf{a}_\nu$ being selected is given by [32]

$$p_{\nu}^{\text{torn}} = \frac{1}{\mu^q} \left((\mu - \nu + 1)^q - (\mu - \nu)^q \right) \tag{16}$$

For the work presented here, tournament selection is carried out with $q = 3$, and the population size $\mu = 100$. The reason for evaluating two selection routines is based on consideration for the transmitter hardware requirements. Tournament selection does not require proportional fitness assignments as in (15), and uses a lower population reducing the memory overhead. However, tournament selection is considerably more exploitative in nature, losing 50% of the solutions through the selection process alone [34], possibly finding a non-optimal solution. Results from both selection routines are presented to illustrate the difference in channel control performance.

Crossover imitates the principles of natural reproduction, and is applied with a probability, $\rho_c = 0.7$ to randomly-selected individuals chosen by the either of the selection routines. Both algorithms apply a double point, $m = 2$ crossover, that was implemented by generating two unique random integers in the range $\{1, \ldots, I - 1\}$, which are subsequently sorted into ascending order, followed by simply exchanging the substrings between the successive cross over points. Mutation was originally developed as a background operator [30], able to introduce new genetic

material into the search routine such that the probability of evaluating a solution in Φ_g will never be zero. Mutation is performed on each individual scaling factor, $a_i \in \mathbf{a}_\nu \forall \nu \in \{1, \ldots, \mu\}$, with a probability $\rho_m = 0.05$ for SUS and with $\rho_m = 0.1$ for the tournament selection. If a given scaling factor a_i is chosen for mutation, it is simply replaced by another randomly-generated number in the set $\{0, 0.01, \ldots, 1\}$. The precedent for the choice of both double point, as supposed to single point cross over, and the choice of random mutation was determined from [14] where theses sub-routine variables were empirically adjusted to determine their effects upon optimisation ability.

Some feedback loop must exist that passes back information regarding the effectiveness of a solution at each generation. In this work, at the 'proof of concept' stage, the simulation will return the DC gain at each receiver location to the fitness function. In a practical system it is envisaged to use one of two methods'. Firstly the receiver, or more precisely transceiver, returns the DC gain or SNR, using a supervisory audio tone similar to GSM techniques, or secondly, if this optimisation process has been simulated in many scenarios, and the best and worst case powers are known, the transceiver can simply return a 'too high' or 'too low' command, informing the transmitter some change should be made to the power ratios. Either method could be applied as and when needed, or within some predefined protocol sequence, and would be suitable when one or many receivers are present. Moreover, both methods are applicable to scenarios when users enter or leave the room, since, in theory, they too have the same receiver design that requires the same power distribution to operate.

In general, a GA is run over many generations until the algorithm converges, or the result has satisfied some defined solution criteria. According the previously published work, [14], 5000

generations were found to be suitable when applied to both algorithms. As an indication of the time required for each of the GAs to converge, and to reaffirm the difference in speed between the use of SUS and T3 selection routines where the later does not require proportional fitness assignments, the simulations were implemented in Matlab running on a 3 GHz Intel Pentium 4 machine. The time required to complete the 5000 generation optimisation for the SUS based GA was approximately 2 min, however for the T3 based GA this time was reduced to just 40 s. Given the operating system overhead and program footprint incurred my Matlab to complete the simulations, it is envisaged that for the final practical realisation based upon a micro-controller, the T3 based GA convergence time can be reduced to near real time whilst the SUS based GA will converge within a few seconds of a user adjusting their position.

5 Results

5.1 Optimisation of an Empty Environment

To begin detailing the GA optimisation effectiveness, firstly consider the system deployment environment to be an empty room with width $x = 6\,\text{m}$, depth $y = 6\,\text{m}$ and height $z = 3\,\text{m}$, where the ceiling and walls have a reflectivity coefficient $\rho = 0.75$, and the floor has a reflectivity coefficient $\rho = 0.3$. Upon the ceiling, 25 uniformly-distributed diffusion spots are formed, and 1024 single element receivers, each with a $\text{FOV}_{\mathcal{R}} = 55°$, and active collection area of $A_{\mathcal{R}} = 0.0001\,\text{m}^2$ are uniformly distributed over the room at a height of $z = 1\,\text{m}$ with alignment statistics as described in section 2.1. The resultant received power distribution can be seen in Figure 2(a). As shown, the received power has a range between 19.9 µW and 56.7 µW, a deviation of 36.8 µW, or 65% of the peak value. Furthermore, the bandwidth, as in Figure 2(c) varies between 14.6 MHz and 65.9 MHz, whilst the RMS delay spread, shown in Figure 2(e) varies between 0.73 ns and 2.17 ns.

Important factors to note are the peaks and valleys within the received power distribution of Figure 2(a). This is due to each receiver being aligned differently to ones at adjacent positions. This variability, that is not only present from one environment to the next, but also from receiver position within a given environment highlights the challenge which system designers face.

Upon optimisation of the transmitter ratios by application of the SUS based GA, the received power distribution, shown in Figure 2(b), is reduced to a range varying between 10.7 µW and 18.8 µW, a deviation of 8.1 µW, or 43% from the peak value. In comparison to the non-optimised case, and defining the GA optimisation gain to be the improvement as a %, in the power deviation between the non-optimised and optimised distributions, the GA optimisation gain for this scenario is therefore 22%. Considering bandwidth, shown in figure 2(d), the GA has reduced the peak bandwidth found within the room to 53.7 MHz, but the worst case, or guaranteed minimum bandwidth, remains the same as in the non-optimised case at 14.6 MHz. The peak, or worst case RMS delay spread, as shown in figure 2(f), has increased from 2.17 ns to 2.73 ns, a reasonable compromise, given the reduced power deviation the GA has provided.

5.2 Optimisation Including User Movement

Within the established environment, two mobile users were subsequently incorporated. User 1 has a shoulder to shoulder width of 0.7 m, front to back depth of 0.4 m, and height of 1.8 m, and is considered to have a reflectivity of $\rho = 0.3$. User 2 is identical, but with a reduced height of 1.6 m. User 1 and user 2 are simulated to have a movement pattern shown in figures 3 (a) and (c) respectively. Each user is modelled to move sequentially through the 9 positions, and cannot

occupy the same space at the same time.

Figure 4(a) depicts the SUS based and tournament with 3 candidate (T3) selection scheme based GAs for the optimised and non optimised power deviation at each movement position and when empty. It shows the non optimised empty room power deviation is 65% (as per figure 2(a)), which, upon user movement, is perturbed by up to 6%, with a range of 9% between 62% and 71%. After optimisation with the SUS based GA, the empty room deviation is reduced by 22% to 43% (as per figure 2(b)), with the maximum perturbation from user movement being increased 2% to 8%, whilst the range is reduced 3% to 6% as it varies between 44% and 50%. Application of the T3 based GA, yields a reduction in power deviation of 18% to 47%, with the maximum perturbation being reduced 2% to 4%, and the range is reduced 5% to 4% as it varies between 47% and 51%. Figure 4(b) depicts the associated optimised bandwidth (OB), non optimised bandwidth (NOB), optimised RMS delay spread (Orms), and non-optimised RMS delay spread (NOrms), when empty (/E), and with movement (/M), of the system. Here it is shown, similar to the empty case, there is little penalty from applying the GA with $< 2.5\,\text{MHz}$ reduction in bandwidth for the T3 scheme and $< 1.5\,\text{ns}$ RMS delay spread penalty over the users' movement positions.

Finally, to provide further evidence of the ability of the GA to handle multiple dynamic scenarios, a second environment was created., This had the same dimensions as previously but the ceiling, south and west walls had reflectivities increased to $\rho = 0.8$, the east wall reflectivity was reduced to $\rho = 0.6$ and the north wall reflectivity was reduced to $\rho = 0.5$. User 1 and User 2 were then modelled moving in a sequence of 9 positions, as depicted in Figures 3(b) and (d) respectively. Figure 5(a) provides the results of the simulation whereby the non-optimised empty

room power deviation is 73%, which, upon user movement, is perturbed by up to 8%, with a range of 9% between 65% and 74%. After optimisation with the SUS based GA, the empty room deviation is reduced by 27% to 46%, with the maximum perturbation being reduced 3% to 5%, as the range is maintained at 9% as it varies between 42% and 51%. With the application of the T3 based GA, the empty room deviation is reduced by 22% to 51%, with the maximum perturbation being reduced 1% to 7%, as the range is again maintained at 9% as it varies between 44% and 53%. Figure 5(b) provides the associated optimised bandwidth (OB), non-optimised bandwidth (NOB), optimised RMS delay spread (Orms), and non-optimised RMS delay spread (NOrms) when empty (/E), and with movement (/M) of the system. It can be seen that, similar to the case of environment 1, the optimisation produces for the worst case < 2.5 MHz reduction in bandwidth and < 1.5 ns RMS delay spread penalty over the users' movement positions.

6 Conclusions

This paper has demonstrated further the novel approach of using a GA-controlled MSD transmitter, capable of successfully optimising the received power distribution in multiple environments with multiple mobile users, each capable of randomly aligning their receivers. From the evaluation of two tailored GAs, an optimisation gain of up to 27% can be achieved for empty environments, whilst a gain of 26% can be achieved when the users are moving. Furthermore, the user's movement has been shown to be capable of perturbing the power distribution by up to 8%, which can be reduced to 5% upon application of this technique. The optimisation has also been achieved with negligible bandwidth and RMS delay spread penalties, of < 2.5 MHz and < 1.5 ns respectively. Finally, this method has the potential to provide a highly adaptable approach to the problem of channel variability from deployment environment changes, random user

alignment and multiple user movement, in applications where cost and mobility are paramount.

References

[1] Green, R.J., Joshi, H., Higgins, M.D., and Leeson M.S.: 'Recent developments in indoor optical wireless systems.', IET Commun., 2008, 2,(1), pp. 3–10.

[2] Hashemi, H., Yun, G., Kavehrad, M., Behbahani, F., and Galko, P.A.: 'Indoor propagation measurements at infrared frequencies for wireless local area networks applications.' IEEE Trans. Veh. Technol., 1994, 43, (3), pp. 562–576.

[3] Moreira, A.J.C., Valadas, R.T., and de Oliveira Duarte A.M.: 'Optical interference produced by artificial light.', Wireless Networks, 1997, 3, (2), pp. 131–140.

[4] Gfeller, F.R., and Bapst, U.: 'Wireless in-house data communication via diffuse infrared radiation.', Proc IEEE., 1979, 67, (11), pp. 1474–1486.

[5] O'Brien, D.C., Katz, M., Wang, P., Kalliojarvi, K., Arnon, S., et al.: 'Short Range Optical Wireless Communications.', Wireless World Research Forum., 2005.

[6] Djahani, P., and Kahn, J.M.: 'Analysis of infrared wireless links employing multibeam transmitters and imaging diversity receivers.', IEEE Trans. Commun., 2000, 48, (12), pp. 2077–2088.

[7] Ramirez-Iniguez, R., and Green. R.J.: 'Optical antenna design for indoor optical wireless communication systems.', Int. J. Commun. Syst., 2005, 18, (3), pp. 229–245.

[8] Lee, D.C.M., Kahn, J.M., and Audeh, M.D.: 'Trellis-coded pulse-position modulation for indoor wireless infrared communications.', IEEE Trans. Commun., 1997, 45, (9), pp. 1080–1087.

[9] Uno, H., Kumatani, K., Okuhata, H., Shirakawa, I., and Chiba, T.: 'ASK digital demodulation scheme for noise immune infrared data communication.', Wireless Networks, 1997, 3, (2), pp. 121–129.

[10] Dickenson, R.J., and Ghassemlooy, Z.: 'A feature extraction and pattern recognition receiver employing wavelet analysis and artificial intelligence for signal detection in diffuse optical wireless communications.', IEEE Trans. Wireless. Commun., 2003, 10, (2),pp. 64–72.

[11] Wong. D.W.K., Chen, G., and Yao, J.: 'Optimization of spot pattern in indoor diffuse optical wireless local area networks.', Optics Express., 2005, 13, (8), pp.3000–3014.

[12] Wen, M., Yao, J., Wong, D.W.K., and Chen, G.C.K.: 'Holographic diffuser design using a modified genetic algorithm.', Optical Eng., 2005, 44, (8), pp. 085801–8.

[13] Kirkpatrick, S., Gelatt, C.D., and Vecchi, M.P. 'Optimization by Simulated Annealing.', Science., 1983, 220, (4598), pp. 671–680.

[14] Higgins, M.D., Green, R.J., and Leeson, M.S.: 'A Genetic Algorithm Method for Optical Wireless Channel Control.', IEEE J. Lightwave. Tech., 2009, 27, (6), pp. 760–772.

[15] Higgins, M.D., Green, R.J., and Leeson, M.S.: 'Genetic Algorithm Channel Control for Indoor Optical Wireless Communications.', Int. Conf. on Transparent Optical Networks - ICTON, Athens, Greece, June 2008, vol. 4, . pp. 189–192.

[16] Higgins, M.D., Green, R.J., and Leeson, M.S.: 'Receiver alignment dependence of a GA controlled optical wireless transmitter.', J. of Optics A: Pure and Applied Optics., 2009, 11, (7), pp. 075403.

[17] Kahn, J.M., Krause, W.J., and Carruthers, J.B.: 'Experimental characterization of non-directed indoor infrared channels.', IEEE Trans. Commun., 1995, 43, (234), pp. 1613–1623.

[18] Yang, H., and Lu, C.: 'Infrared wireless LAN using multiple optical sources.', IEE Proc. Optoelectron., 2000, 147, (4), pp. 301–307.

[19] Jivkova, S., Hristov, B.A., and Kavehrad, M.: 'Power-efficient multispot-diffuse multiple-input-multiple-output approach to broad-band optical wireless communications.', IEEE Trans. Veh. Technol., 2004, 53, (3), pp. 882–889.

[20] O'Brien, D.C., Faulkner, G.E., Zyambo, E.B., Jim, K., Edwards, D.J., et al.: 'Integrated transceivers for optical wireless communications.', IEEE J. Sel. Topics Quantum Electron., 2005, 11, (1), pp. 173–183.

[21] Pohl, V., Jungnickel, V., and von Helmolt, C.: 'Integrating-sphere diffuser for wireless infrared communication.', IEE Proc. Optoelectron., 2000. 147, (4), pp. 281–285.

[22] Komine, T., and Nakagawa, M.: 'Fundamental analysis for visible-light communication system using LED lights.', IEEE Trans. Consum. Electron., 2004, 50, (1), pp. 100–107.

[23] Barry, J.R., Kahn, J.M., Krause, W.J., Lee, E.A., and Messerschmitt, D.G.: 'Simulation of multipath impulse response for indoor wireless optical channels.', IEEE J. Sel. Areas. Commun., 1993, 11, (3), pp. 367–379.

[24] Carruthers, J.B., Carroll, S.M., and Kannan, P.: 'Propagation modelling for indoor optical wireless communications using fast multi-receiver channel estimation.', IEE Proc. Optoelectron., 2003, 150, (5), pp. 473–481.

[25] Carruthers, J.B, and Kannan, P.: 'Iterative site-based modelling for wireless infrared channels.', IEEE Trans. Antennas. Propag., 2002, 50, (5), pp. 759–765.

[26] Carruthers, J.B., and Kahn, J.M.: 'Modeling of nondirected wireless infrared channels.', IEEE Trans. Commun., 1997, 45, (10). pp. 1260–1268.

[27] Haratcherev, I., Taal, J., Langendoen, K., Lagendijk, R., and Sips, H.: 'Automatic IEEE 802.11 rate control for streaming applications.', Wireless Commun. Mob. Comput., 2005, 5, (4), pp. 421–437.

[28] Garcia-Zambrana, A., and Puerta-Notario, A.: 'Novel approach for increasing the peak-to-average optical power ratio in rate-adaptive optical wireless communication systems.', IEE Proc. Optoelectron., 2003, 150, (5), pp. 439–444.

[29] Pakravan, M.R., and Kavehrad, M.: 'Indoor wireless infrared channel characterization by measurements.', IEEE Trans. Veh. Technol., 2001, 50, (4), pp. 1053–1073.

[30] Bäck, T., Hammel, U., and Schwefel, H.P.: 'Evolutionary Computation: Comments on the History and Current State.', IEEE Trans. Evol. Comput., 1997, 1, (1), pp. 3–17.

[31] Rothlauf, F.: 'Representations for genetic and evolutionary algorithms.', Springer, 2002.

[32] Bäck, T.: 'Evolutionary algorithms in theory and practice : evolution strategies, evolutionary programming, genetic algorithms.', Oxford University Press, 1996.

[33] Baker, J.E.: 'Reducing bias and inefficiency in the selection algorithm.', Proc. 2nd Int. Conf. Genetic Algorithms, Cambridge, MA, 1987, pp. 14–21.

[34] Poli, R.: 'Tournament Selection, Iterated Coupon-Collection Problem, and Backward-Chaining Evolutionary Algorithms.', in Wright, A.H. (Ed.): 'Foundations of Genetic Algorithms',(Springer 2005), pp. 132–155.

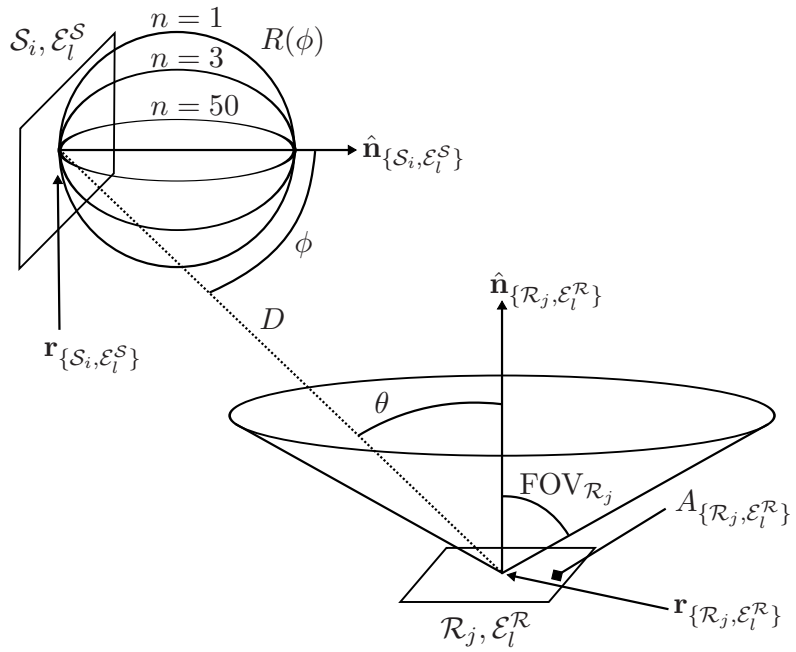

Figure 1: Source, receiver and reflector geometry, adapted from [23].

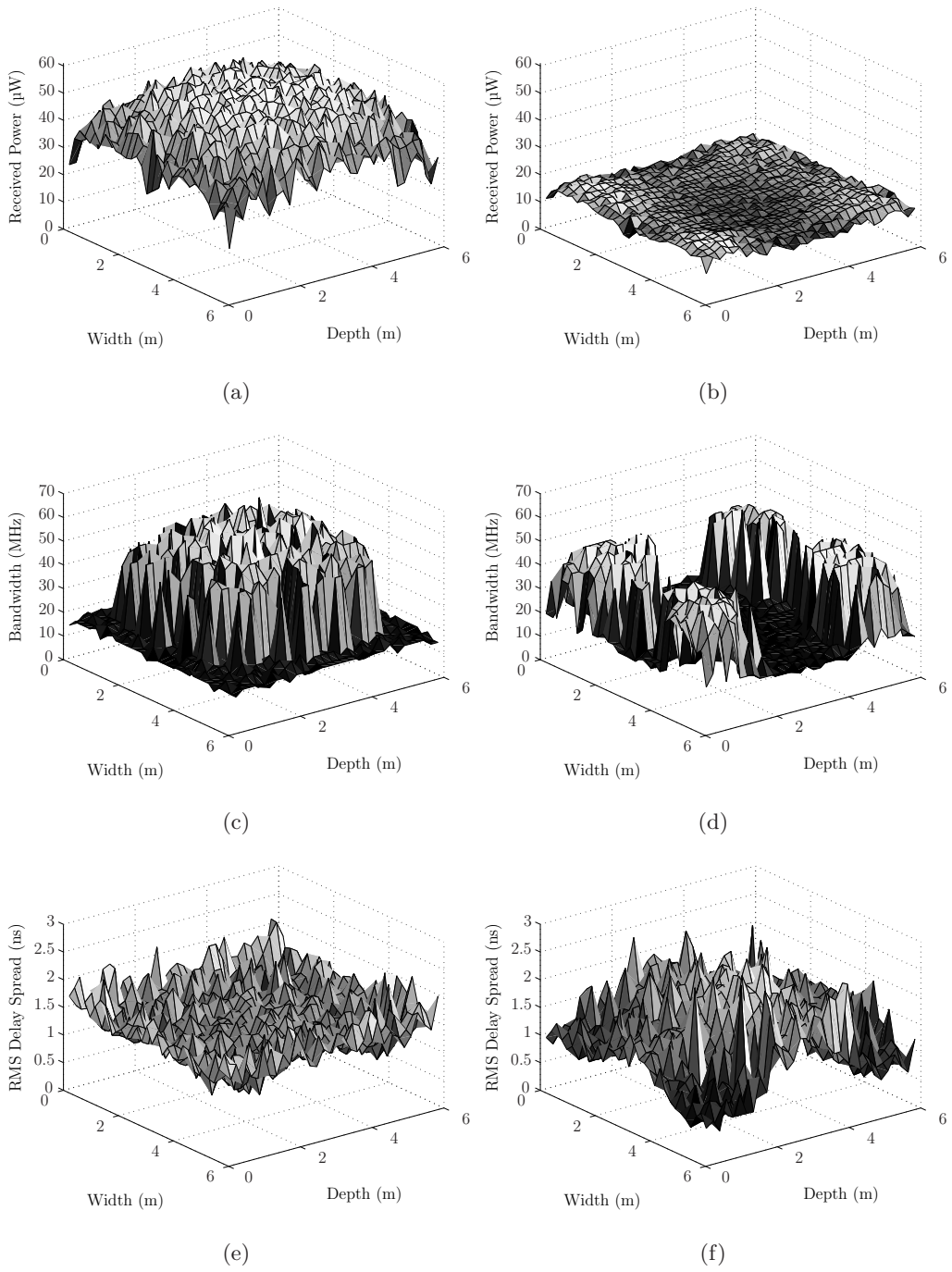

Figure 2: Optimisation random receiver alignment using the SUS based GA. Power: (a)non optimised, (b) optimised. Bandwidth: (c) non optimised, (d) optimised. RMS delay spread: (e) non optimised, (f) optimised.

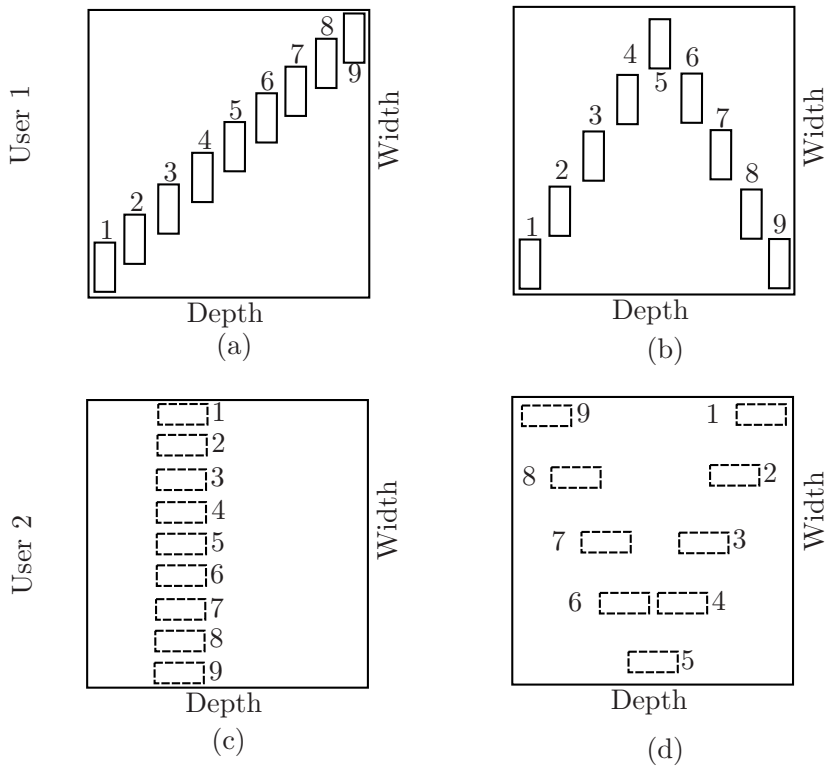

Figure 3: Movement positions of 2 users. (a) User 1, movement pattern 1. (b) User 1, movement pattern 2. (c) User 2, movement pattern 3. (d) User 2, movement pattern 4.

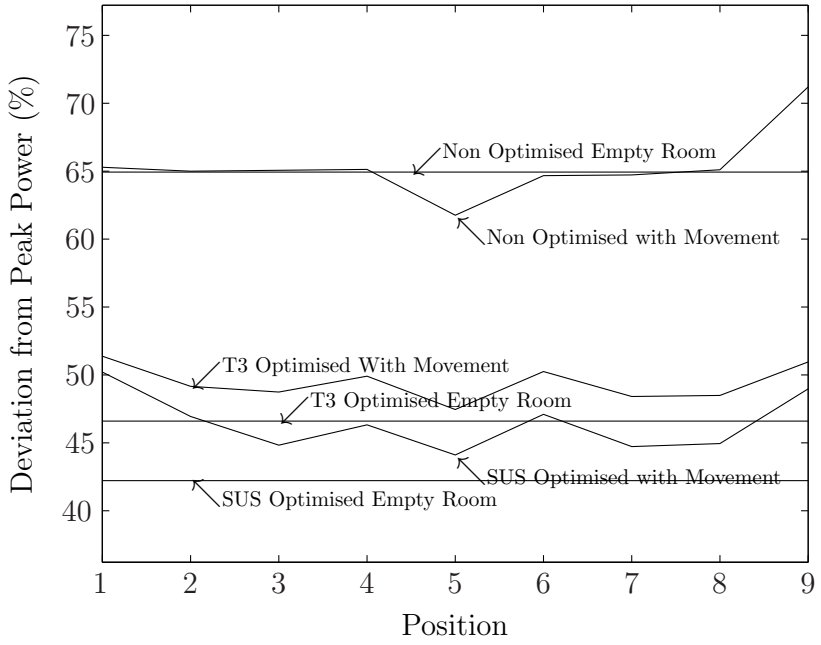

(a)

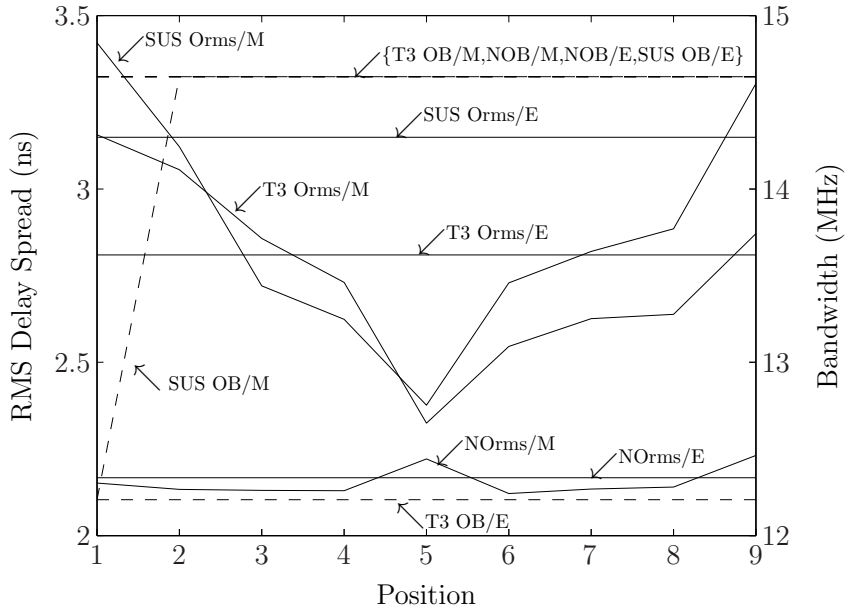

(b)

Figure 4: Environment 1 multi user optimisation (a) Power deviation. (b) Bandwidth (- -) and RMS delay spread (–).

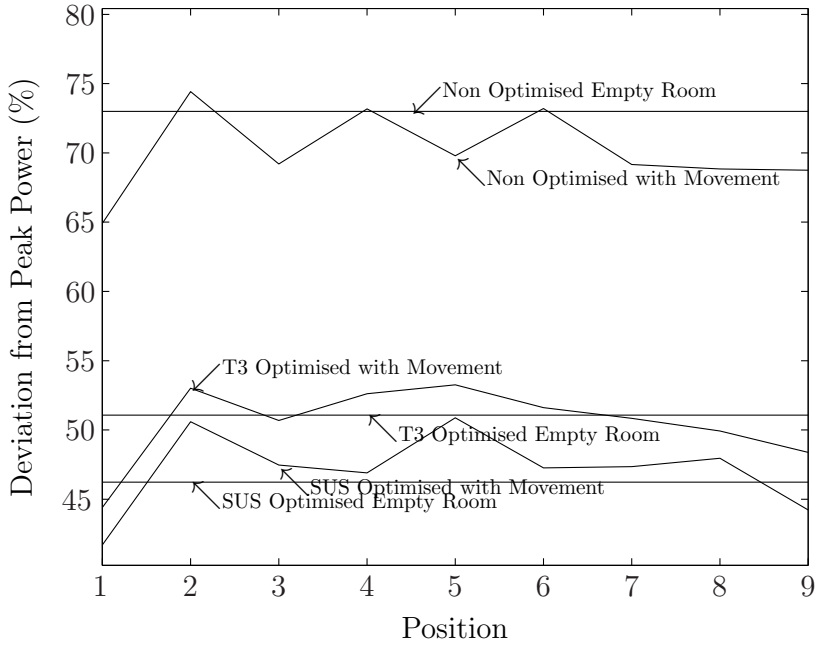

(a)

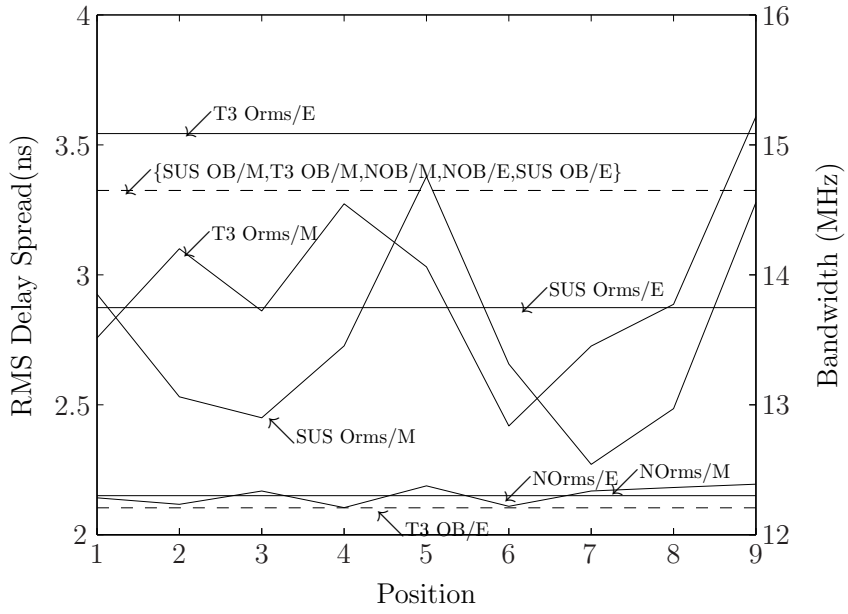

(b)

Figure 5: Environment 2 multi user optimisation (a) Power deviation. (b) Bandwidth (- -) and RMS delay spread (–).